Extended model of noninteger-dimensional space for anisotropic solids with q-deformed derivatives

José Weberszpil [1,*] and Ralf Metzler [2,†]

[1] *Federal Rural University of Rio de Janeiro, UFRRJ-DEFIS/ICE, BR-465, Km 7 Seropédica-Rio de Janeiro, CEP 23.897-000, Brazil*

[2] *Institute of Physics and Astronomy, University of Potsdam, Karl-Liebknecht-Straße 24/25, 14476 Potsdam-Golm, Germany*

(Received 14 April 2026; accepted 30 July 2026; published 18 August 2026)

We propose a noninteger-dimensional spatial model for anisotropic solids incorporating a q-deformed derivative operator inspired by the Tsallis nonadditive entropy framework. This generalization provides a unified and flexible analytical formalism for exploring anisotropic thermal properties. We derive explicit expressions for the electronic and phonon densities of states and for the phonon specific heat, showing how the Hausdorff dimension α and the deformation parameter q affect the spectral and thermodynamic response. The model is applied to several solid-state materials and provides a close description of their measured specific-heat behavior over broad temperature ranges. The fitted results illustrate the ability of the regularized entropic formulation to describe departures from the standard Debye response. Finally, we relate the q-deformation qualitatively to disorder-controlled conformable kinetics, suggesting a possible connection to microscopic heterogeneity and effective memory signatures without assuming a universal quantitative relation between q and the kinetic exponent μ.

DOI: 10.1103/m98w-77xg

I. INTRODUCTION

Anisotropic materials exhibit direction-dependent physical properties that fundamentally challenge conventional thermodynamic models based on three-dimensional isotropic model approaches [1–3]. These materials, ranging from layered van der Waals crystals [4,5] to nanostructured composites [6,7], demonstrate thermal transport phenomena that cannot be adequately described by classical Debye theory alone [2,8]. The directional asymmetries in such systems often arise from underlying microstructural heterogeneities, crystalline anisotropy, or topological constraints that effectively reduce the dimensionality of phonon propagation [9–12].

In 1990, He proposed a groundbreaking framework to address this challenge by mapping anisotropic systems to effectively isotropic entities embedded in a noninteger-dimensional space (NIDS) characterized by a Hausdorff dimension α [13]. This geometric approach provides a mathematically elegant method to encode anisotropic effects through dimensional reduction, enabling the application of conventional statistical mechanics to complex materials with modified density of states (DOS).

However, many anisotropic solids often exhibit additional complexities beyond simple dimensional reduction. Many materials display nonlinear thermal responses, memory effects, and correlations that suggest deviations from extensive thermodynamic behavior [14–16]. These phenomena are particularly pronounced in nanostructured materials [17], where surface effects, quantum confinement, and structural disorder introduce nontrivial statistical signatures [18,19].

Recent advances in our microscopic understanding of q-deformed derivative operators [20–27] and other deformed derivatives, such as conformable derivatives [28], have demonstrated their effectiveness in modeling systems with anomalous diffusion, non-Gaussian fluctuations, and nonextensive behavior. Building on this theoretical foundation, the present work extends He's noninteger-dimensional framework by incorporating q-deformed derivatives inspired by Tsallis' nonadditive entropy formalism [14].

The q-deformed derivative operator was defined as

$$D_q[f](x) = [1 + (1 - q)x]\frac{df}{dx} \tag{1}$$

by Borges in the context of nonextensive thermostatistics [29]. In the original construction, x is dimensionless. In the present context, x denotes a suitably scaled frequency or energy variable, such as ω/ω_0 or βE, so the factor $[1 + (1 - q)x]$ remains dimensionless and does not affect the units of the resulting physical observable.

This deformed derivative offers a systematic way to incorporate nonlinear corrections that effectively encode nonlocal interactions and memory effects, as typically encountered in complex materials. In the limit $q \to 1$, the operator reduces to the ordinary derivative, guaranteeing consistency with standard thermodynamic descriptions. Moreover, the q-deformed operator D_q furnishes a convenient framework for modeling systems in which anisotropy depends explicitly on position or energy. Examples include quantum wells and superlattices with engineered anisotropy [30,31], fractals and hierarchically

*Contact author: josewebe@gmail.com

†Contact author: ralf.metzler@uni-potsdam.de

Published by the American Physical Society under the terms of the Creative Commons Attribution 4.0 International license. Further distribution of this work must maintain attribution to the author(s) and the published article's title, journal citation, and DOI.

structured materials such as silica aerogels and porous silicon [32,33], nanocomposites with interface-dominated transport [17], and materials exhibiting non-Debye phonon behavior [11].

The combination of a noninteger-dimensional space embedding with q deformation creates a unified analytical framework capable of describing both geometric anisotropy and statistical nonextensivity within a single mathematical formalism. As will be shown in the present work, this approach enables closed-form expressions for modified DOS and specific heat capacity that can be directly validated against experimental data.

Classical Debye and He's fractional-dimensional approaches capture much of the low temperature behavior, but anomalous transport and memory effects in complex solids require the use of tools such as continuous-time random walks (CTRWs) and/or fractional Fokker-Planck equation (FFPE) dynamics. For a comprehensive background on anomalous diffusion and fractional dynamics we refer to the reviews [19,34]. The memory-induced anomalous response discussed here is consistent with the CTRW/fractional kinetics and FFPE paradigm.

II. DEFORMED THERMODYNAMIC MODEL IN NONINTEGER-DIMENSIONAL SPACE

Following He's original approach [13], an anisotropic medium can be mapped onto an isotropic system embedded in a noninteger-dimensional space with Hausdorff dimension α.

The q-deformed derivative operator employed here is closely related to those previously discussed in the context of anomalous diffusion and generalized entropy production [20,21,23,24]. These earlier formulations demonstrated how such operators encode effective thermodynamic deformation and memory effects in a variety of physical settings.

A. Noninteger-dimensional embedding with deformed derivatives

We reinterpret the momentum-space measure and excitation statistics in terms of q-deformed calculus [20,29]. In the Hausdorff-conformal approach, the derivative operator acting on a function f may be written as

$$D_\alpha[f](k) = \Omega_\alpha k^{\alpha-1}\frac{df}{dk}, \quad \Omega_\alpha = \frac{2\pi^{\alpha/2}}{\Gamma(\alpha/2)}, \tag{2}$$

where $k = |\mathbf{k}|$ is the magnitude of the wave vector in momentum space. The factor $k^{\alpha-1}$ is the radial weight induced by the hyperspherical surface measure in α-dimensional space [13,35,36]. This construction is consistent with the Hausdorff-measure formalism for noninteger-dimensional spaces and with the axiomatic framework of noninteger-dimensional integration [13,35,37,38]. We note that foundational aspects of noninteger-dimensional space theory can be traced back to the seminal work by Stillinger [35], which established the mathematical framework for noninteger-dimensional calculus in physical systems.

Recent developments have considerably broadened the mathematical and physical scope of NIDS methods. Balankin and Mena examined vector differential operators in fractional-dimensional spaces, on fractal sets, and in fractal continuum models, thereby clarifying the relationships and distinctions between these different representations of fractal media [39]. More recently, Tarasov formulated a self-consistent calculus in NIDS, including scalar and vector differential operators, volume, surface, and line integrals, as well as differential forms and NIDS generalizations of the fundamental theorems of calculus [40]. This formulation provides a systematic mathematical basis for treating differentiation and integration as mutually consistent operations in spaces of noninteger dimension.

The NIDS framework has also been extended to general fractional calculus. In this construction, the usual one-dimensional integral and differential operators entering general fractional calculus are replaced by their NIDS counterparts, and the corresponding fundamental theorems are established for an admissible class of general fractional operators [41]. This development distinguishes the noninteger dimensionality of the underlying space from the noninteger order and nonlocality of fractional operators.

Recent applications further demonstrate the breadth of this approach. A generalization of equilibrium thermodynamics to a space of thermodynamic states with noninteger dimension has been proposed using differential forms in NIDS [42]. In continuum mechanics, a fractal theory of thermoelasticity has been developed in a noninteger-dimensional space, combining NIDS vector operators with generalized heat conduction and memory-dependent thermoelastic response [43]. Although the present work requires only the radial NIDS measure and the associated mode-counting structure, these recent advances provide the broader mathematical and physical context within which our deformed thermodynamic model is situated.

In the condensed-matter setting, this type of noninteger-dimensional description is also consistent with fractional-dimensional models for anisotropic solids.

Radial meaning of k and origin of the factor $k^{\alpha-1}$

Throughout this work, $k := |\mathbf{k}| \geqslant 0$ denotes the radial magnitude in an α-dimensional (generally noninteger) isotropic momentum space. Accordingly, the Hausdorff measure in hyperspherical coordinates reads

$$d^\alpha k \;=\; S_{\alpha-1}\, k^{\alpha-1}\, dk, \quad S_{\alpha-1} = \frac{2\pi^{\alpha/2}}{\Gamma(\alpha/2)}, \tag{3}$$

where $S_{\alpha-1}$ is the surface area of the unit $(\alpha-1)$-sphere, so the factor $k^{\alpha-1}$ is the usual radial Jacobian in α dimensions. Because k is by definition nonnegative (radial coordinate), no absolute value $|k|^{\alpha-1}$ is required in (3). If one were to write the measure in Cartesian components over $\mathbb{R}^\alpha$, the integrand is rotation-invariant and the reduction to radial integration yields exactly the factor $k^{\alpha-1}$.

In this sense, the factor $k^{\alpha-1}$ is not an *ad hoc* ingredient but the Jacobian associated with isotropic mode counting in Hausdorff dimension α, consistent with the fraction-dimensional construction used by [13] and the general noninteger-dimensional calculus framework [35].

B. Comparison between the noninteger-dimensional-space derivative and the q-deformed derivative: Distinct roles and mathematical self-consistency

1. Distinct physical roles of the NIDS and q-deformed operators

The NIDS construction and the q-deformed derivative act on distinct physical sectors of the model and should therefore be regarded as complementary rather than interchangeable descriptions. The NIDS parameter α modifies the geometry of the accessible momentum space through the radial measure, Eqs. (3), and consequently determines the leading power-law dependence of the density of states. It primarily describes dimensional reduction, anisotropic mode accessibility, and geometrical constraints on phonon or electronic propagation. By contrast, the Borges operator D_q, Eq. (1), introduces a scale-dependent deformation with respect to the dimensionless energy or frequency variable x. Its role is not to replace the noninteger-dimensional measure but to describe departures from the undeformed statistical and kinetic response at fixed geometrical dimension. Such departures may originate from spatial heterogeneity, distributed kinetic coefficients, correlated relaxation, or coarse-grained disorder. In this interpretation, the local q-deformation represents an effective macroscopic remnant of more complex microscopic dynamics; a microscopic route by which quenched disorder and heterogeneous kinetic coefficients generate such deformed dynamics and power-law memory kernels is discussed in Sec. III E and Ref. [28].

The distinction can be seen directly from the density of states. Let ε denote the dimensionless energy measured from the threshold. The NIDS construction alone gives, apart from geometrical prefactors, $g_\alpha(\varepsilon) \propto \varepsilon^{\alpha/2-1}$. Application of the q-deformed derivative instead produces

$$g_{\alpha,q}(\varepsilon) = g_\alpha(\varepsilon)[1 + (1-q)\varepsilon] \propto \varepsilon^{\alpha/2-1} + (1-q)\varepsilon^{\alpha/2}, \quad (4)$$

which is precisely the structure already obtained, with the full dimensional prefactors, in Eq. (19). Varying α changes the geometrical scaling exponent, whereas varying q introduces an additional energy-dependent contribution without changing the underlying NIDS geometry. The second term in Eq. (4) cannot, over a finite energy interval, be reproduced by merely replacing α with another effective dimension because it generates a superposition of two different powers rather than a single modified power law. The same separation appears in the thermal response, Eq. (47): the first term is the NIDS Debye contribution, controlled by the geometrical parameter α, while the second is the genuinely q-dependent correction. Consequently, α characterizes the effective geometry of the mode space, whereas q characterizes the additional statistical or kinetic deformation occurring within that geometry, and the limit $q \to 1$ removes this additional correction, recovering the original NIDS formulation.

2. Self-consistency and the role of the deformed integral

The Borges construction [29] also defines a formal q-deformed integral, the operational inverse of D_q:

$$\mathcal{I}_q[f](x) := \int \frac{f(x)}{1 + (1-q)x}\, dx. \quad (5)$$

Direct substitution confirms that the two classical fundamental theorems of calculus—relating differentiation and integration as mutually inverse operations—hold exactly for this pair of operators, namely,

$$D_q[\mathcal{I}_q[f]](x) = f(x), \quad (6)$$

and

$$\mathcal{I}_q[D_q[f]](x) = f(x) + \text{const}, \quad (7)$$

so $(D_q, \mathcal{I}_q)$ is mathematically self-consistent, in exact analogy with the ordinary derivative/integral pair recovered in the limit $q \to 1$.

Despite this consistency, $\mathcal{I}_q$ is deliberately not used when constructing the cumulative counting functions $G(E)$, Eq. (15), and $G_p(\omega)$, Eq. (23). These are obtained from the standard (undeformed) integration of the Hausdorff measure $d^\alpha k$, Eqs. (3), because they represent a purely geometric mode-counting problem in NIDS momentum space, for which the relevant deformation is already fully encoded in α. To express the deformation in terms of dimensionless variables, we define $\widehat{G}(\varepsilon) := G(E_0 + E_r\varepsilon)$, with $\varepsilon = (E - E_0)/E_r$, and $\widehat{G}_p(\widetilde{\omega}) := G_p(\omega_0\widetilde{\omega})$, with $\widetilde{\omega} = \omega/\omega_0$. The q deformation is then applied only once, at the differentiation step that converts the cumulative mode count into the physically observable densities of states, $g_q(E) = \frac{1}{E_r} D_q[\widehat{G}](\varepsilon)$ and $g_{p,q}(\omega) = \frac{1}{\omega_0} D_q[\widehat{G}_p](\widetilde{\omega})$, as derived explicitly below in Eqs. (19) and (37). This is the step at which nonadditive/memory corrections physically act, since it is the density of states—not the raw geometric count—that enters the thermal averages defining $U(T)$ and $C_V(T)$. Applying $\mathcal{I}_q$ a second time when building $G(E)$ itself would double count the statistical deformation and spoil the clean $q \to 1$ recovery of He's undeformed NIDS result (Sec. II F). Self-consistency of the present construction therefore follows both from the formal identities (6) and (7) and from the physically motivated, single, well-defined point at which the deformation enters.

C. Physical interpretation of the q-deformed framework

The introduction of q-deformed derivatives in the context of anisotropic solids requires careful physical interpretation to justify its application beyond mere mathematical formalism. The deformation parameter q encodes deviations from extensive statistical behavior that arise naturally in systems with:

Geometric constraints. In materials with fractal or hierarchical microstructures, the effective phase space accessible to excitations becomes restricted. The q deformation captures this reduced accessibility through a position-dependent weighting of the derivative operator, effectively encoding the geometric constraints imposed by the material's internal structure [13,37].

Correlation and scale-dependent effects. Anisotropic materials often exhibit long-range correlations arising from directional bonding, layered structures, or coherent interfaces. The factor $[1 + (1-q)x]$ in Eq. (1) introduces an energy- or frequency-scale-dependent weighting of the local response, thereby providing an effective description of correlation-induced departures from the undeformed behavior [14,20]. Since the Borges q derivative is local in the variable x, this factor does not, by itself, generate an explicit temporal memory

kernel. Rather, when the q deformation is interpreted as the coarse-grained manifestation of heterogeneous microscopic dynamics, it may encode effective signatures of correlations and memory whose underlying nonlocal structure resides in the corresponding microscopic or mesoscopic dynamics [28]. Therefore, the term "scale-dependent effects" is more precise here than either memorylike effects or spacelike effects.

Interface and surface contributions. In nanostructured anisotropic materials, surface and interface effects become significant. The q deformation naturally accounts for these contributions by modifying the DOS in an energy-dependent manner, reflecting the altered vibrational spectrum near interfaces [17,44].

Non-Debye phonon behavior. Many anisotropic materials exhibit phonon dispersion relations that deviate from the linear Debye approximation. The q-deformed DOS captures these deviations through its nonlinear energy dependence, providing a phenomenological description of complex phonon interactions.

The mathematical structure of the q-deformed framework ensures that these physical effects are encoded in a thermodynamically consistent manner. The approach preserves fundamental thermodynamic relationships while allowing for systematic deviations from extensive behavior, making it particularly suitable for modeling real materials with complex internal structures. In Ref. [28], the reader can find more detailed explanation on microscopic origins of deformed derivative and its connection [20].

Applications of Tsallis nonextensive statistical mechanics have demonstrated remarkable success in describing systems with long-range correlations, multifractal structures, and memory effects [15,16,45,46]. The framework has been particularly effective in condensed matter systems exhibiting power-law distributions, anomalous diffusion, and non-Gaussian fluctuations [47,48]. In this context we note that the use of q-deformed calculus (including q derivatives) and the broader nonadditive-entropy framework has been developed [29] and applied extensively beyond the original Tsallis proposal [14].

Broader context: mesoscopic foundations and analogous complex materials

The broader relevance of the Borges q-calculus employed here is supported by related developments in nonextensive dynamics. Nobre *et al*. proposed nonlinear generalizations of the Schrödinger, Klein–Gordon, and Dirac equations that admit q-exponential traveling-wave solutions whilst preserving the usual energy–momentum relation and recovering the corresponding linear equations in the limit $q \to 1$. Although those nonlinear equations do not employ precisely the Borges operator used in the present work, they demonstrate that q-deformed differential structures arise naturally in quantum and relativistic descriptions rather than being restricted to phenomenological curve fitting [49].

At the mesoscopic level, Deppman *et al*. established a formal connection between a Boltzmann equation endowed with a nonadditive correlation functional and a nonlinear Fokker–Planck equation associated with nonadditive entropy. In that construction, the q algebra enters through the collision term and the conventional Boltzmann and Fokker–Planck descriptions are smoothly recovered when $q \to 1$. This result does not constitute a direct microscopic derivation of the particular Borges derivative adopted here; nevertheless, it provides an important kinetic and mesoscopic context in which q represents correlations and departures from Boltzmann–Gibbs statistics [50].

A physically instructive parallel is also provided by the extensive body of work of Reis, Oliveira, and coworkers on manganites [51–58], a class of complex colossal-magnetoresistance materials for which q-statistical concepts have been employed to describe magnetic and thermodynamic properties. These systems are characterized by competing interactions, structural and magnetic heterogeneity, and responses extending over several spatial and energetic scales. They therefore provide a natural analog of the anisotropic and heterogeneous solids considered in the present work.

Within this interpretation, the Hausdorff parameter α and the nonadditivity parameter q need not represent redundant descriptions. Rather, they may encode complementary manifestations of the underlying complexity: α characterizes the effective geometry and the restrictions imposed on the accessible mode space, whereas q characterizes correlated statistical or kinetic departures from the undeformed response. This complementary role is consistent with the distinction between geometrical and q-dependent contributions discussed above. The present framework may therefore provide a route toward extending noninteger-dimensional modeling to complex magnetic solids, including manganites and related structurally heterogeneous materials.

D. Derivation of the cumulative number of states in noninteger-dimensional space

To determine the cumulative number of quantum states $G(E)$ up to a given energy E in a noninteger-dimensional space of Hausdorff dimension α, we proceed as follows.

The number of quantum states with wave-vector magnitude less than k is given by [3,13,35,59]

$$G(E) = \frac{1}{(2\pi)^\alpha} \int_{|\vec{k}| \leqslant k(E)} d^\alpha k, \tag{8}$$

where $d^\alpha k$ denotes the infinitesimal volume element in momentum space with Hausdorff dimension α.

The volume of a hypersphere of radius k in α dimensions is [60–62]

$$\int_{|\vec{k}| \leqslant k} d^\alpha k = \frac{2\pi^{\alpha/2}}{\Gamma(\alpha/2)} \int_0^k k'^{\alpha-1} dk' = \frac{2\pi^{\alpha/2}}{\Gamma(\alpha/2)} \frac{k^\alpha}{\alpha}. \tag{9}$$

Therefore, the cumulative number of states becomes

$$G(E) = \frac{1}{(2\pi)^\alpha} \frac{2\pi^{\alpha/2}}{\Gamma(\alpha/2)} \frac{1}{\alpha} k(E)^\alpha, \tag{10}$$

Origin and combination of the (2π) factors

The factors of (2π) appearing in the expressions for $G(E)$ and $g(E)$ (below) have two distinct origins: (i) the standard phase-space normalization $(2\pi)^{-\alpha}$ (one factor of 2π per dimension in α dimensions), and (ii) the hyperspherical surface factor $S_{\alpha-1} = 2\pi^{\alpha/2}/\Gamma(\alpha/2)$ coming from the reduction of

the α-dimensional integral to radial coordinates in noninteger dimension. Thus, schematically,

$$G(E) \propto \frac{1}{(2\pi)^\alpha}\int d^\alpha k = \frac{1}{(2\pi)^\alpha} S_{\alpha-1}\int_0^{k(E)} k^{\alpha-1}dk,$$

so all (2π) factors could, in principle, be absorbed into a single geometric prefactor. In the present work, we prefer to keep the (2π) factors explicit to make transparent the standard phase-space normalization and the separate geometric contribution from the NIDS hyperspherical surface.

To express k as a function of energy, we use the free-particle dispersion relation:

$$E = E_0 + \frac{\hbar^2 k^2}{2m} \Rightarrow k(E) = \sqrt{\frac{2m}{\hbar^2}(E - E_0)}, \tag{11}$$

where E_0 is the minimum (threshold) energy. Thus,

$$k^\alpha = \left(\frac{2m}{\hbar^2}\right)^{\alpha/2}(E - E_0)^{\alpha/2}. \tag{12}$$

Substituting into the expression for $G(E)$, we obtain

$$G(E) = \frac{1}{(2\pi)^\alpha}\frac{2\pi^{\alpha/2}}{\Gamma(\alpha/2)}\frac{1}{\alpha}\left(\frac{2m}{\hbar^2}\right)^{\alpha/2}(E - E_0)^{\alpha/2}. \tag{13}$$

Grouping constants and using the abbreviation, we define

$$C_\alpha = \frac{1}{(2\pi)^\alpha}\frac{2\pi^{\alpha/2}}{\Gamma(\alpha/2)}\frac{1}{\alpha}\left(\frac{2m}{\hbar^2}\right)^{\alpha/2} \tag{14}$$

to arrive at the expression[1]

$$G(E) = C_\alpha (E - E_0)^{\alpha/2}. \tag{15}$$

E. Electronic density of states

From the cumulative distribution of states, Eq. (15), we obtain the undeformed electronic DOS in a noninteger-dimensional space by differentiating

$$g(E) = \frac{dG}{dE} = C_\alpha \frac{\alpha}{2}(E - E_0)^{\alpha/2-1}. \tag{16}$$

Substituting the explicit form of C_α, we get

$$g(E) = \frac{1}{(2\pi)^\alpha}\frac{2\pi^{\alpha/2}}{\Gamma(\alpha/2)}\frac{1}{2}\left(\frac{2m}{\hbar^2}\right)^{\alpha/2}(E - E_0)^{\alpha/2-1}. \tag{17}$$

In accordance with the dimensionless energy variable introduced in Eq. (4), we define

$$\varepsilon := \frac{E - E_0}{E_r}, \tag{18}$$

where E_r is a fixed characteristic reference-energy scale. It may be chosen, for example, as a representative excitation-energy or bandwidth scale and does not alter the leading noninteger-dimensional power-law dependence of the density of states.

[1]In [13], the symbol $G_\epsilon(E)$ denotes the electronic DOS. In the present work, we adopt the notation $g_q(E)$ to clearly emphasis its origin from the application of the q-deformed derivative operator to the cumulative number of states, $G(E)$.

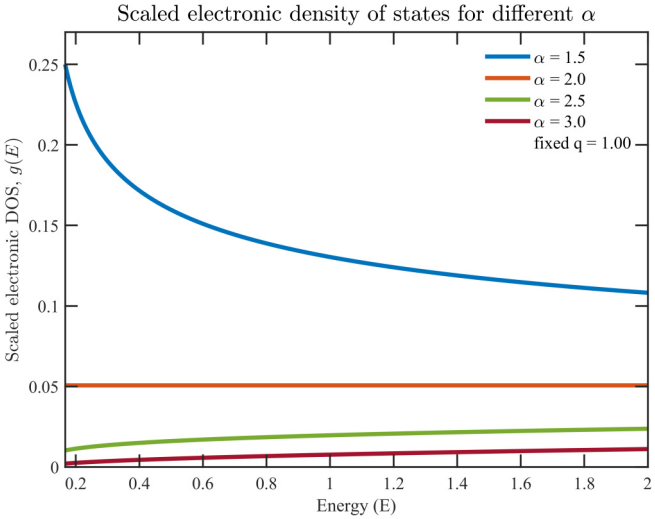


FIG. 1. Scaled electronic density of states for different values of the fractal dimension α, with $q = 1$. The curves are plotted slightly away from the threshold E_0 to prevent the integrable near-edge divergence for $\alpha < 2$ from dominating the linear-scale visualization.

Now, instead of the standard derivative, we apply the q-deformed derivative, Eq. (1), to the cumulative distribution expressed in terms of the dimensionless variable ε, $\widehat{G}(\varepsilon) := G(E_0 + E_r\varepsilon)$. We then obtain

$$g_q(E) := \frac{1}{E_r}D_q[\widehat{G}](\varepsilon) = C_\alpha\frac{\alpha}{2}(E - E_0)^{\frac{\alpha}{2}-1}\left[1 + (1 - q)\frac{E - E_0}{E_r}\right]. \tag{19}$$

Accordingly, the argument entering the Borges deformation factor is dimensionless and is written as $1 + (1 - q)\varepsilon = 1 + (1 - q)(E - E_0)/E_r$.

Hence, the full expression for the DOS becomes

$$g_q(E) = \frac{1}{(2\pi)^\alpha}\frac{2\pi^{\alpha/2}}{\Gamma(\alpha/2)}\frac{1}{2}\left(\frac{2m}{\hbar^2}\right)^{\alpha/2} \times (E - E_0)^{\alpha/2-1}\left[1 + (1 - q)\frac{(E - E_0)}{E_r}\right]. \tag{20}$$

This rigorous derivation is built up without any empirical correction factors, clearly establishing the deformation as naturally arising from the mathematical structure of the generalized derivative.

As seen in Fig. 1, depending on the magnitude of α both concave and convex forms are possible. Figure 1 also illustrates the electronic DOS as a function of energy for different values of the noninteger dimension parameter α. The inferred dimension $\alpha < 3$ implies reduced phase-space accessibility, consistent with phonon scattering suppression and dimensional crossover phenomena, commonly observed in low-dimensional or anisotropic solids [9–11,13,63–65]. This behavior is consistent with the geometric interpretation of Hausdorff dimension applied to anisotropic or fractal media, as proposed in He's model [13].

F. Recovery of He's original result ($q \to 1$ limit)

In the limit $q \to 1$, the q-deformed derivative D_q reduces to the ordinary derivative. Therefore, the deformed DOS (19) reduces to the standard noninteger-dimensional DOS,

$$g_{q=1}(E) = \frac{dG(E)}{dE} = \frac{1}{(2\pi)^\alpha}\frac{S_{\alpha-1}}{\alpha}\frac{d}{dE}[k(E)^\alpha] \propto (E - E_0)^{\alpha/2-1}, \tag{21}$$

with $S_{\alpha-1} = 2\pi^{\alpha/2}/\Gamma(\alpha/2)$ and the free-particle dispersion $k(E) = \sqrt{2m(E-E_0)}/\hbar$. This is precisely the same scaling and prefactor structure obtained in He's fraction-dimensional mapping of anisotropic solids to an isotropic α-dimensional system [13]. We thus keep the notation $g_{q=1}(E)$ and no additional volumelike quantity V_α is required: all geometric information is already encoded in the Hausdorff measure and the normalization $(2\pi)^{-\alpha}$.

III. PHONON DENSITY OF STATES IN NONINTEGER-DIMENSIONAL SPACE

We now consider the number of vibrational (phonon) modes with frequency less than or equal to ω, but in a noninteger-dimensional momentum space of Hausdorff dimension α.

The number of modes is then given by

$$G_p(\omega) = \frac{1}{(2\pi)^\alpha}\int_{|\vec{k}|\le k(\omega)} d^\alpha k, \tag{22}$$

where $k(\omega) = \omega/v_s$ and v_s is the speed of sound.

Using the volume of an α-dimensional ball, Eq. (9), we obtain

$$G_p(\omega) = \frac{1}{(2\pi)^\alpha}\frac{2\pi^{\alpha/2}}{\Gamma(\alpha/2)}\frac{1}{\alpha}\left(\frac{\omega}{v_s}\right)^\alpha. \tag{23}$$

The phonon density of states is given by the derivative of this result, i.e.,

$$g_p(\omega) = \frac{dG_p}{d\omega} = \frac{1}{(2\pi)^\alpha}\frac{2\pi^{\alpha/2}}{\Gamma(\alpha/2)}\left(\frac{1}{v_s}\right)^\alpha \omega^{\alpha-1}. \tag{24}$$

Equation (24) includes the classical Debye form in the limit $\alpha = 3$. For general α, it defines the spectral distribution of phonon modes in fractal media.

Figure 2 presents the phonon DOS modified by the q-deformed framework. As q deviates from unity, the deformation primarily affects the intermediate-to-high reduced-frequency regime, whereas the leading low-frequency power-law remains controlled by the Hausdorff dimension α. This deformation is associated with systems exhibiting correlations, constraints, or generalized statistics in the Tsallis formalism [14].

Throughout the q-dependent phonon expressions, the argument of the Borges deformation is the dimensionless reduced frequency

$$\widetilde{\omega} := \frac{\omega}{\omega_0}, \tag{25}$$

where ω is the physical angular frequency and ω_0 is a fixed reference frequency. Accordingly, the deformation factor is understood as

$$1 + (1-q)\widetilde{\omega} = 1 + (1-q)\frac{\omega}{\omega_0}, \tag{26}$$

so both q and the quantity multiplying $(1-q)$ are dimensionless.

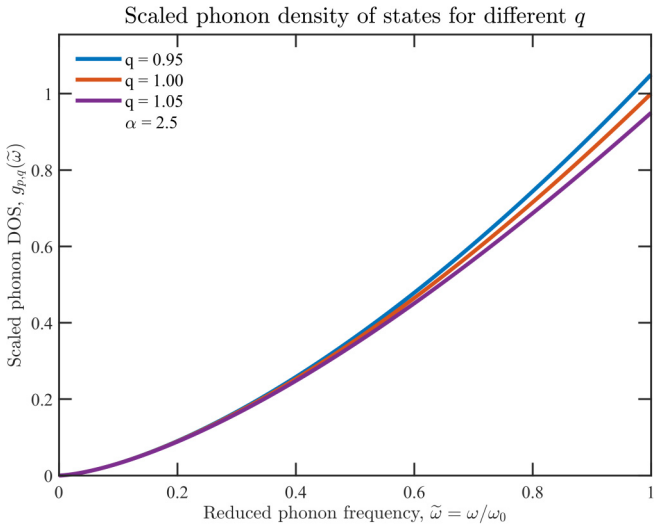


FIG. 2. Phonon DOS for different q-deformations as a function of the reduced frequency $\widetilde{\omega} = \omega/\omega_0$, with $\alpha = 2.5$.

A. Low-frequency behavior and log-scale representation

The q-deformed phonon DOS shown in Fig. 2 and derived below has the general structure

$$g_{p,q}(\omega) \propto \omega^{\alpha-1}\left[1 + (1-q)\frac{\omega}{\omega_0}\right], \tag{27}$$

with the fractal Hausdorff dimension α and the deformation parameter q. For $\omega \to 0$, we have

$$1 + (1-q)\frac{\omega}{\omega_0} = 1 + \mathcal{O}\left(\frac{\omega}{\omega_0}\right), \tag{28}$$

so the leading low-frequency behavior is

$$g_{p,q}(\omega) \sim \omega^{\alpha-1}, \quad (\omega \to 0), \tag{29}$$

independent of q to leading order. On a log-log plot, this implies that the low-frequency slope is the same for all q and is equal to $(\alpha - 1)$, while the q dependence only produces subleading corrections that become visible at larger ω (or, equivalently, at higher temperatures once folded with the Bose factor). Therefore, the low-ω part of the curves in Fig. 2 remain almost unchanged when q is varied, and the main effect of the deformation appears in the intermediate-to-high frequency regime. In other words, the low-ω part is expected to remain almost identical across q in a log-log representation, consistent with the interpretation that q primarily controls higher-energy deviations from the Debye-like spectrum.

B. Specific heat in the standard Debye approach

We evaluate the internal energy associated with phonon modes in a medium of fractional Hausdorff dimension α,

$$U(T) = \int_0^{\omega_D} \hbar\omega g_p(\omega) n_B(\omega, T)\, d\omega, \tag{30}$$

where $g_p(\omega)$ is the phonon DOS, $n_B(\omega, T) = 1/(e^{\hbar\omega/k_BT} - 1)$ is the Bose-Einstein distribution, and ω_D is the (temperature-independent) Debye cutoff frequency.

In the previous section, we derived the DOS in noninteger-dimensional space, given by Eq. (24),

$$g_p(\omega) = \frac{1}{(2\pi)^\alpha} \frac{2\pi^{\alpha/2}}{\Gamma(\alpha/2)} \left(\frac{1}{v_s}\right)^\alpha \omega^{\alpha-1}, \tag{31}$$

where v_s is the speed of sound.

We change variables to $x = \hbar\omega/k_BT$, so $\omega = \frac{k_BT}{\hbar}x$ and $d\omega = \frac{k_BT}{\hbar}dx$. The internal energy becomes

$$\begin{aligned} U(T) &= \frac{1}{(2\pi)^\alpha} \frac{2\pi^{\alpha/2}}{\Gamma(\alpha/2)} \left(\frac{1}{v_s}\right)^\alpha \int_0^{\omega_D} \frac{\hbar\omega^\alpha}{e^{\hbar\omega/k_BT} - 1} d\omega \\ &= \left(\frac{k_BT}{\hbar}\right)^{\alpha+1} \frac{1}{(2\pi)^\alpha} \frac{2\pi^{\alpha/2}}{\Gamma(\alpha/2)} \left(\frac{1}{v_s}\right)^\alpha \hbar \\ &\quad \times \int_0^{T_D/T} \frac{x^\alpha}{e^x - 1} dx, \end{aligned} \tag{32}$$

where $T_D = \hbar\omega_D/k_B$ is the Debye temperature.

In the low-temperature limit $T \ll T_D$, the upper limit of the integral tends to infinity, and the integral can be evaluated as [66,67]

$$\int_0^\infty \frac{x^\alpha}{e^x - 1} dx = \Gamma(\alpha + 1)\zeta(\alpha + 1), \tag{33}$$

where $\zeta(s)$ is the Riemann zeta function.

Therefore, the internal energy and the specific heat scale as

$$U(T) \propto T^{\alpha+1} \Rightarrow C_V(T) = \frac{dU}{dT} \propto T^\alpha. \tag{34}$$

This confirms that in a space with Hausdorff dimension α, the specific heat scales with temperature as T^α at low temperatures.

C. Specific heat with deformed phonon density of states in a noninteger-dimensional space

To include nonlinear effects in the phonon statistics, we express the cumulative phonon mode distribution in terms of the dimensionless reduced-frequency variable as

$$\widehat{G}_p(\widetilde{\omega}) := G_p(\omega_0\widetilde{\omega}), \quad \widetilde{\omega} := \frac{\omega}{\omega_0}.$$

Applying the q-deformed derivative to this representation, we obtain

$$\begin{aligned} g_{p,q}(\omega) &:= \frac{1}{\omega_0} D_q[\widehat{G}_p](\widetilde{\omega}) = \frac{1}{\omega_0}[1 + (1-q)\widetilde{\omega}] \frac{d\widehat{G}_p}{d\widetilde{\omega}} \\ &= [1 + (1-q)\widetilde{\omega}] \frac{dG_p}{d\omega} = \left[1 + (1-q)\frac{\omega}{\omega_0}\right] \frac{dG_p}{d\omega}, \end{aligned} \tag{35}$$

since

$$\frac{d\widehat{G}_p}{d\widetilde{\omega}} = \omega_0 \frac{dG_p}{d\omega}.$$

Computing the derivative,

$$\frac{dG_p}{d\omega} = \frac{1}{(2\pi)^\alpha} \frac{2\pi^{\alpha/2}}{\Gamma(\alpha/2)} \left(\frac{1}{v_s}\right)^\alpha \omega^{\alpha-1}, \tag{36}$$

we obtain

$$g_{p,q}(\omega) = \frac{1}{(2\pi)^\alpha} \frac{2\pi^{\alpha/2}}{\Gamma(\alpha/2)} \left(\frac{1}{v_s}\right)^\alpha \omega^{\alpha-1} \left[1 + (1-q)\frac{\omega}{\omega_0}\right]. \tag{37}$$

Here, $\widetilde{\omega} = \omega/\omega_0$ is the reduced frequency defined above.

After the change of variables $x = \hbar\omega/(k_BT)$, the q-dependent contribution becomes

$$(1-q)\frac{k_BT}{\hbar\omega_0} x. \tag{38}$$

The constant factor $1/\omega_0$ is retained throughout the derivation of the q-dependent contribution and is subsequently incorporated into the corresponding effective coefficient. Hence, the specific-heat expression derived below preserves the same temperature dependence employed in the numerical analysis. Since the coefficient multiplying the q-dependent term is treated as an independent fitting parameter, the explicit introduction of the reference frequency ω_0 requires no modification of the numerical fitting functions or of the reported parameter values, while q remains a dimensionless nonadditivity parameter.

Now, the internal energy becomes

$$U_q(T) = \int_0^{\omega_D} \hbar\omega \cdot g_{p,q}(\omega) \cdot \frac{1}{e^{\hbar\omega/k_BT} - 1} d\omega. \tag{39}$$

Using the change of variables $x = \hbar\omega/k_BT$ and $\omega = \frac{k_BT}{\hbar}x$, we obtain

$$\begin{aligned} U_q(T) &= \frac{1}{(2\pi)^\alpha} \frac{2\pi^{\alpha/2}}{\Gamma(\alpha/2)} \left(\frac{1}{v_s}\right)^\alpha \left(\frac{k_BT}{\hbar}\right)^{\alpha+1} \hbar \\ &\quad \times \int_0^{T_D/T} \frac{x^\alpha \left[1 + (1-q)\frac{k_BT}{\hbar\omega_0}x\right]}{e^x - 1} dx, \end{aligned} \tag{40}$$

where $T_D = \hbar\omega_D/k_B$ is the Debye temperature.

As in the undeformed derivation above, in the low-temperature Debye regime, $T \ll T_D$, the upper limit T_D/T is large and may be extended to infinity.

Separating the terms inside the integral, we obtain

$$\begin{aligned} U_q(T) = AT^{\alpha+1} \Bigg[&\int_0^\infty \frac{x^\alpha}{e^x - 1} dx + (1-q)\frac{k_BT}{\hbar\omega_0} \\ &\times \int_0^\infty \frac{x^{\alpha+1}}{e^x - 1} dx \Bigg], \end{aligned} \tag{41}$$

where the prefactor A is defined as

$$A = \frac{1}{(2\pi)^\alpha} \frac{2\pi^{\alpha/2}}{\Gamma(\alpha/2)} \left(\frac{1}{v_s}\right)^\alpha \hbar \left(\frac{k_B}{\hbar}\right)^{\alpha+1}, \tag{42}$$

and using the standard integral

$$\int_0^\infty \frac{x^\mu}{e^x-1}dx = \Gamma(\mu+1)\zeta(\mu+1), \tag{43}$$

we obtain for the internal energy

$$U_q(T) = AT^{\alpha+1}\Bigg[\Gamma(\alpha+1)\zeta(\alpha+1) + (1-q)\frac{k_BT}{\hbar\omega_0}\Gamma(\alpha+2)\zeta(\alpha+2)\Bigg]. \tag{44}$$

Differentiating with respect to T, the specific heat becomes

$$\begin{aligned} C_{V,q}(T) &= \frac{dU_q}{dT} \\ &= A(\alpha+1)\Gamma(\alpha+1)\zeta(\alpha+1)T^\alpha + A(1-q)\frac{k_B}{\hbar\omega_0} \\ &\quad\times[(\alpha+2)\Gamma(\alpha+2)\zeta(\alpha+2)T^{\alpha+1}]. \end{aligned} \tag{45}$$

In the limit $q\to 1$, Eq. (45) reduces to the undeformed fractional-dimensional Debye form

$$\begin{aligned} C_V^{(D,\alpha)}(T) &:= \lim_{q\to1} C_{V,q}(T) \\ &= A(\alpha+1)\Gamma(\alpha+1)\zeta(\alpha+1)\,T^\alpha \\ &\equiv A_1T^\alpha. \end{aligned} \tag{46}$$

Therefore, the q-deformed specific heat can be written as

$$C_{V,q}(T) = C_V^{(D,\alpha)}(T) + A_2(1-q)T^{\alpha+1}, \tag{47}$$

showing explicitly that the deformation introduces a temperature-dependent correction governed by $(1-q)T^{\alpha+1}$.

Here, we have defined the constants A_1, A_2 as

$$A_1 := A(\alpha+1)\Gamma(\alpha+1)\zeta(\alpha+1), \tag{48}$$

$$A_2 := A\frac{k_B}{\hbar\omega_0}(\alpha+2)\Gamma(\alpha+2)\zeta(\alpha+2). \tag{49}$$

Since the factor $1/\omega_0$ is included explicitly in the definition of A_2, the specific-heat expressions below require no additional explicit factor of ω_0.

D. Factorization of the deformed specific heat expression

From the full derivation of the deformed phonon specific heat, we obtained Eq. (45) along with the prefactor (42).

Then the specific heat can be written in the form

$$C_{V,q}(T) = A_1T^\alpha + A_2(1-q)T^{\alpha+1}, \tag{50}$$

which can also be factorized as

$$C_{V,q}(T) = T^\alpha[A_1 + A_2(1-q)T]. \tag{51}$$

It is important to note that this expression has physically meaningful prefactors, derived from the deformed Debye model in noninteger-dimensional space.

E. High-temperature regularization and the role of the cutoff term

For a conventional monatomic crystalline solid, the complete Debye model approaches the classical Dulong–Petit limit at sufficiently high temperature [3],

$$C_V(T) \to 3R, \tag{52}$$

where R is the gas constant. By contrast, the low-temperature expression in Eq. (51), when extrapolated beyond its original regime of validity, may grow without bound.

To regularize this high-temperature growth, we introduce the phenomenological factor [28]

$$\frac{1}{1+(T/T_D)^n}, \tag{53}$$

where $T_D > 0$ defines an effective thermal crossover scale and $n > 0$ controls the strength and sharpness of the regularization. Within the present model, T_D should not necessarily be identified with an independently measured bulk Debye temperature.

For $T \ll T_D$, the regularization factor admits the expansion

$$\left[1+\left(\frac{T}{T_D}\right)^n\right]^{-1} = 1-\left(\frac{T}{T_D}\right)^n + \mathcal{O}\left[\left(\frac{T}{T_D}\right)^{2n}\right], \tag{54}$$

so the correction is algebraically small and the leading low-temperature power-law dependence is preserved.

For $T \gg T_D$, the regularization factor behaves as

$$\left[1+\left(\frac{T}{T_D}\right)^n\right]^{-1} \sim \left(\frac{T_D}{T}\right)^n. \tag{55}$$

Consequently, the complete regularized specific heat has the high-temperature asymptotic form

$$C_{V,q}(T) \sim A_1T_D^nT^{\alpha-n} + A_2(1-q)T_D^nT^{\alpha+1-n}. \tag{56}$$

The denominator therefore suppresses the nonregularized growth but does not, by itself, universally impose an asymptotically constant specific heat. When the q-dependent contribution dominates, an approximately constant high-temperature response requires $n \simeq \alpha+1$. If $n < \alpha+1$, the fitted response retains a residual increase, whereas $n > \alpha+1$ produces a decreasing asymptotic contribution.

Physical interpretation of the regularization exponent n

The condition $n > 0$ ensures that the regularization factor decreases monotonically as T/T_D increases. The exponent n is treated as an effective phenomenological fitting parameter and controls the sharpness of the thermal crossover. Smaller values produce a smoother and broader crossover, whereas larger values produce a sharper suppression of the non-regularized power-law growth.

No universal quantitative relation between n and phonon anharmonicity follows from the present model alone. The fitted values should therefore be interpreted together with α, q, and the temperature interval covered by each dataset. For six of the seven systems considered here, the fitted values satisfy $n \simeq \alpha+1$, yielding an approximately level high-temperature response. The cobalt nanowire composite is the main exception and retains an increasing fitted response over its restricted experimental temperature interval.

Accordingly, the terms high-temperature regularization and thermal crossover are more appropriate than *saturation* as universal descriptions of the factor in Eq. (53).

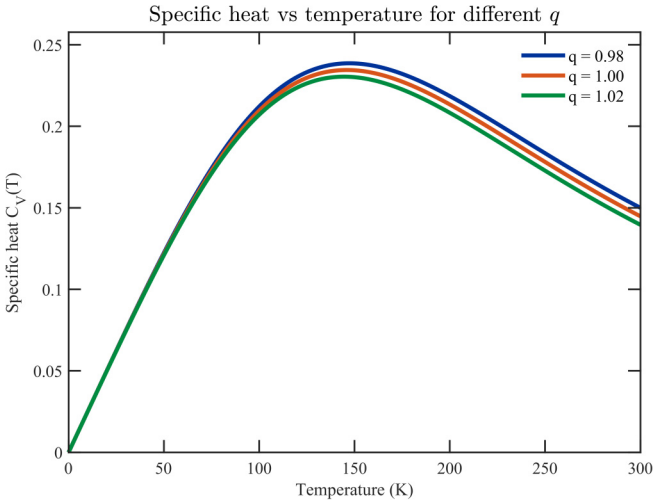


FIG. 3. Specific heat $C_{V,q}(T)$ versus temperature T for different values of q, obtained from Eq. (57) with $\alpha = 1.0$, $T_D = 180\,\mathrm{K}$, and $n = 2.8$ (with fixed $A_1 = 2.5 \times 10^{-3}$ and $A_2 = 1.5 \times 10^{-5}$).

The final expression, which we refer to as the entropic model, is given by

$$C_{V,q}(T) = T^{\alpha}[A_1 + A_2(1-q)\,T]\left(1 + \left(\frac{T}{T_D}\right)^{n}\right)^{-1}. \quad (57)$$

We note that the term *entropic model* is employed here to emphasize the role of the nonextensive entropy parameter q, which modulates the system's deviation from classical extensive thermodynamics. The presence of the deformation encodes thermodynamic anomalies often observed in complex or anisotropic materials.

Figure 3 shows the temperature dependence of the specific heat $C_{V,q}(T)$ for different values of the entropic parameter q, as computed from Eq. (57). For $q = 1$, the model recovers the undeformed Debye-like reference behavior. Small deviations from $q = 1$ produce systematic shifts in the magnitude and curvature of the heat-capacity curves, especially in the intermediate-to-high temperature regime, while preserving the low-temperature power-law scaling controlled by α. In this sense, the parameter q may be interpreted as encoding weak nonextensive effects associated with disorder, heterogeneity, or finite-size constraints in anisotropic solids. The coefficients A_1 and A_2, defined in Eqs. (48) and (49), together with n, were selected as representative phenomenological parameters satisfying the constraints of the model and yielding a physically reasonable crossover profile. In particular, A_1 sets the overall amplitude, A_2 controls the strength of the q-dependent correction, and n determines the smoothness of the thermal crossover near T_D.

F. Microscopic origin of the q deformation and link to conformable dynamics

Recent developments [28] show how quenched disorder and temperature-dependent kinetics produce emergent conformable dynamics. In this framework, the local kinetic coefficient obeys

$$\Gamma(\mathbf{r}, T) = \Gamma_0\, T^{1-\mu}\, f(\mathbf{r}), \quad 0 < \mu < 1, \quad \langle f \rangle = 1, \quad (58)$$

and the thermal evolution may be written in terms of the conformable (local) derivative of a function $\psi(T)$,

$$D_T^{(\mu)}\psi := T^{\,1-\mu}\,\frac{d\psi}{dT}, \quad (59)$$

which captures memory/heterogeneity without explicit nonlocal kernels. After coarse-graining, fluctuations of Γ generate an effective memory kernel with a power-law tail,

$$K(\tau) \sim \tau^{\mu-1}, \quad (60)$$

consistent with non-Markovian relaxation. Such power-law kernels and the associated non-Markovian response are standard hallmarks of anomalous transport based on CTRWs or fractional kinetics [18,19]. Here $K(\tau)$ denotes the effective memory kernel, where $\tau = t - t' > 0$ is the lag time. It quantifies how strongly past states at time t' contribute to the present dynamics at time t after coarse-graining over the fluctuations of Γ. In this representation, the emergence of a power-law tail (60), indicates algebraically decaying memory and is therefore consistent with non-Markovian relaxation.

Under suitable coarse-graining conditions, the conformable kinetic exponent μ may be related to an effective entropic deformation parameter q through a model-dependent mapping,

$$q = \mathcal{Q}(\mu; \mathcal{M}), \quad (61)$$

where $\mathcal{M}$ denotes the set of material-specific microscopic parameters. The functional form of $\mathcal{Q}$ cannot be inferred from conformable scaling alone and requires an independent microscopic derivation and material-specific calibration. In the present work, the conformable description is therefore interpreted as a qualitative microscopic motivation for the q deformation rather than as a parameter-free quantitative prediction of the fitted values of q.

IV. COMPARISON OF THE q-DEFORMED MODEL WITH EXPERIMENTAL DATA

In this section, we compare the proposed q-deformed model for the specific heat $C_{V,q}(T)$ in anisotropic solids by testing it against two experimental datasets from the literature: Sapphire ($\alpha - Al_2O_3$) data taken from [68] and reported by [69] and macroscopic Cobalt nanowire composites as reported in [17].

A. Justification for using C_p data in C_V modeling

Although the model is formulated for the constant-volume specific heat, $C_V(T)$, the experimental datasets considered here are reported as constant-pressure specific heats, $C_p(T)$. These datasets comprise sapphire, quartz, germanium, antimony, bismuth, bismuth silicate, and the cobalt nanowire composite.

The two quantities are related by [3,59]

$$C_p - C_V = \frac{TV\alpha_V^2}{\kappa_T}. \quad (62)$$

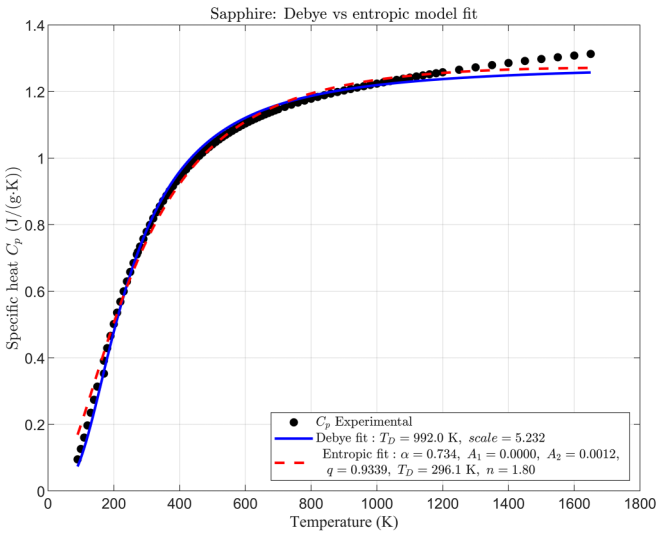


FIG. 4. Specific-heat data for sapphire ($\alpha-Al_2O_3$) compared with the Debye benchmark and the entropic model, Eq. (57). The corresponding best-fit parameters are reported in the plot legend. All experimental data reproduced in this and the following figures can be found in this repository [73].

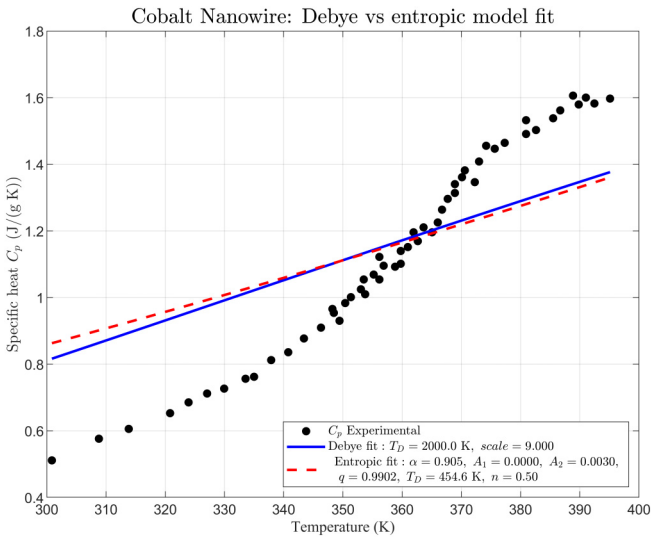


FIG. 5. Specific-heat data for the cobalt nanowire composite compared with the Debye benchmark and the entropic model, Eq. (57). The corresponding best-fit parameters are reported in the plot legend.

Here $\alpha_V := (1/V)(\partial V/\partial T)_P$ is the volumetric thermal expansion coefficient, κ_T is the isothermal compressibility, and V is the molar volume.[2]

For many crystalline solids, the difference between C_p and C_V is modest at low and intermediate temperatures, although it may become appreciable at higher temperatures. In the present phenomenological analysis, $C_p(T)$ is therefore used as an effective proxy for $C_V(T)$ with this approximation kept in mind, particularly for the high-temperature sapphire data.

B. Fit to sapphire specific heat data

The dataset from Ref. [69] covers a wide temperature range, extending from approximately 90 K to 1650 K. We fitted the experimental data using the q-deformed model in a noninteger-dimensional space and compared the result with a Debye benchmark, as shown in Fig. 4. Both models reproduce the main temperature dependence of the measured specific heat, although the entropic model provides a closer description of the low-temperature onset, the intermediate-temperature curvature, and the gradual high-temperature variation.

The parameters of the entropic model should be interpreted as effective phenomenological quantities. The exponent α characterizes the effective power-law scaling associated with the noninteger-dimensional description, q quantifies the departure from the additive limit, T_D defines an effective thermal crossover or regularization scale, and n controls the sharpness of this crossover. The corresponding best-fit parameters are reported in the plot legend.

For the sapphire dataset, the fitted coefficient A_1 reaches its lower bound, indicating that the two amplitude contributions are not independently identifiable within the present paremetrization. Accordingly, the individual fitted coefficients should be interpreted with caution, even though the combined model provides an accurate description of the measured temperature dependence.

C. Fit to cobalt nanowire composite data

The cobalt nanowire composite provides a heterogeneous nanostructured test case in which interfaces, finite-size effects, and orientational disorder may influence the thermal response.

The comparison between the Debye benchmark and the regularized entropic model applied to the cobalt nanowire composite (Fig. 5) shows that both fitting forms capture only the smooth overall variation of the measured response. The dataset extracted from Pradhan *et al.* [17] corresponds to the randomly oriented cobalt nanowire composite rather than to bulk crystalline cobalt. Over the measured interval, $300\,\mathrm{K} \leqslant T \leqslant 400\,\mathrm{K}$, neither model fully reproduces the pronounced curvature and increase of the experimental data. The fitted parameters for both models are reported in the plot legend.

The entropic formulation provides an alternative regularized parametrization through its power-law, deformation, and crossover terms, but no clear superiority over the Debye benchmark can be claimed for this particular dataset without an additional quantitative model comparison. The cobalt nanowire result should therefore be regarded as illustrating both the flexibility and the limitations of the present phenomenological description.

V. THEORETICAL FRAMEWORK AND PARAMETER INTERPRETATION

A. Connection to Tsallis statistical mechanics

The Borges q-deformed derivative employed in this work was introduced in the context of Tsallis nonadditive statistical

[2]We denote the volumetric thermal expansion coefficient by α_V, rather than the more common bare α, to avoid any confusion with the Hausdorff dimension α used throughout this work to characterize the noninteger-dimensional embedding.

mechanics, whose entropy is given by [14,15]

$$S_q = k_B \frac{1 - \sum_i p_i^q}{q - 1}. \tag{63}$$

The associated formalism admits probability distributions with power-law characteristics and provides a possible statistical context for the present deformation. In the phonon problem considered here, the q-dependent DOS is interpreted phenomenologically as representing effective departures from the undeformed response.

Anisotropy, structural disorder, interfaces, and heterogeneous connectivity may generate correlations and non-Debye behavior. However, because the Borges derivative is local in its argument, it does not itself generate an explicit temporal memory kernel. The connection to memory effects arises through the qualitative coarse-grained interpretation discussed in the subsection on the microscopic origin of the q deformation and its link to conformable dynamics.

B. Parameter identifiability and physical constraints

To address concerns about parameter identifiability, we impose physical constraints on the fitting parameters:

Hausdorff dimension $\boldsymbol{\alpha}$. Constrained to $0 < \alpha \leqslant 3$, reflecting the physical requirement that the effective dimensionality cannot exceed the embedding space dimension.

Deformation parameter $\boldsymbol{q}$. In the present fits, the values range from approximately 0.93 to 0.99. They therefore indicate an effectively superadditive deformation of varying strength, while remaining relatively close to the additive limit for most materials.

High-temperature regularization parameters. The parameters T_D and n are constrained to remain positive. Within the present phenomenological model, T_D represents an effective thermal crossover scale and should not necessarily be identified with the independently measured bulk Debye temperature. The exponent n controls the strength of the high-temperature regularization and, together with α and q, determines the asymptotic temperature dependence. When the q-dependent contribution is nonzero, the leading high-temperature behavior is $C_{V,q}(T) \sim T^{\alpha+1-n}$. Therefore, an approximately constant high-temperature response requires $n \simeq \alpha + 1$.

VI. OTHER MATERIALS

To assess the descriptive performance of the modified entropic model for the specific heat capacity, we additionally performed comparative fits against the classical Debye model (see Appendix) across multiple materials with diverse thermal behaviors. Figures 6–10 present the results for germanium, antimony, quartz (SiO_2), bismuth silicate, and bismuth.

In all cases, the experimental data $C_p(T)$ were digitized or obtained from established literature sources: Piesbergen [70] for germanium; Pradhan *et al.* [17] for antimony and bismuth; the NIST Shomate formulation [71] for quartz; and Onderka [72] for bismuth silicate. Each dataset was independently fitted using two approaches:

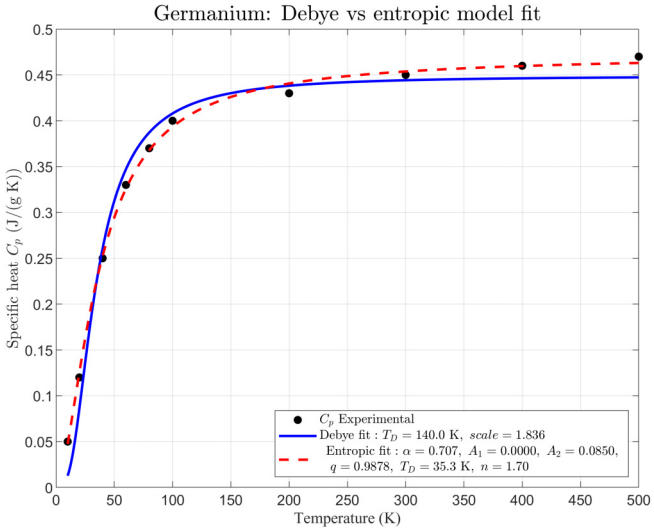


FIG. 6. Specific heat capacity for germanium: Comparison between Debye and entropic model with high-temperature regularization fits. Data from Piesbergen *et al.* (1963) [70]. The corresponding best-fit parameters are reported in the plot legend.

(1) The Debye model, defined by the integral form involving the Debye temperature T_D and an overall scaling factor (see Appendix);

(2) The modified entropic model with high-temperature regularization, Eq. (57), in which α, A_1, A_2, q, T_D, and n control the effective scaling and thermal crossover.

Across these additional materials, both models reproduce the main temperature dependence to varying degrees. In several cases, the regularized entropic model follows the intermediate- and high-temperature curvature more closely, whereas in other temperature intervals the two descriptions are comparable. The degree of improvement is therefore material dependent, and no universal claim of superiority is made. A

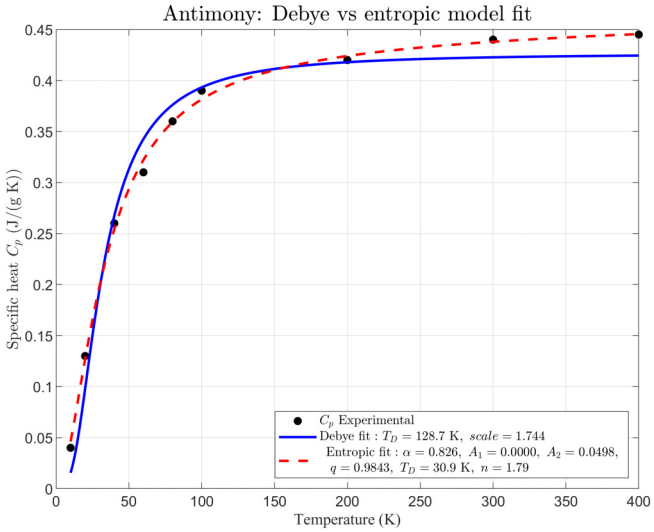


FIG. 7. Specific heat capacity for antimony: Fitting comparison between the Debye model and the modified entropic model. Data from Pradhan [17]. The corresponding best-fit parameters are reported in the plot legend.

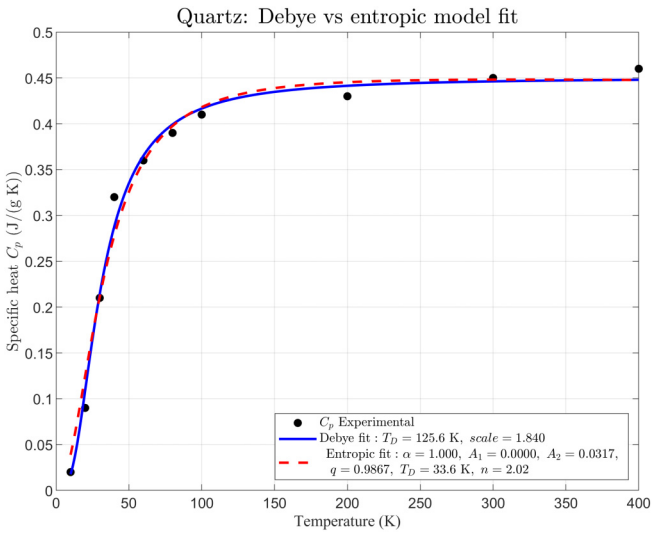


FIG. 8. Specific heat capacity for quartz (SiO_2): Debye and entropic model comparison. Data from NIST standard reference database [71]. The corresponding best-fit parameters are reported in the plot legend.

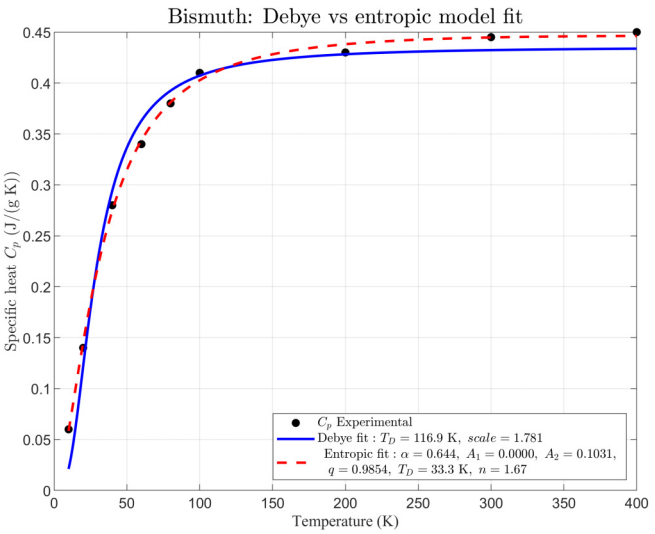


FIG. 10. Specific heat capacity for bismuth: Specific heat fit comparison. Data from Pradhan *et al.* (2008) [17]. The corresponding best-fit parameters are reported in the plot legend.

formal quantitative comparison would require residual analysis, parameter-uncertainty estimates, and information criteria.

These results support the regularized entropic expression as a flexible phenomenological alternative to the Debye benchmark for describing non-Debye specific-heat behavior.

Discussion

The comparative fits demonstrate that the regularized entropic specific-heat expression can reproduce the overall temperature dependence of a range of structurally and thermodynamically distinct materials. The improvement relative to the Debye benchmark is most apparent in cases where the measured response retains appreciable curvature at intermediate and high temperatures. The degree of improvement is nevertheless material dependent. In particular, the cobalt nanowire composite remains a challenging case because its measured response exhibits a pronounced increase over the restricted interval $300\,\mathrm{K} \leqslant T \leqslant 400\,\mathrm{K}$, which is not fully reproduced by either smooth benchmark curve.

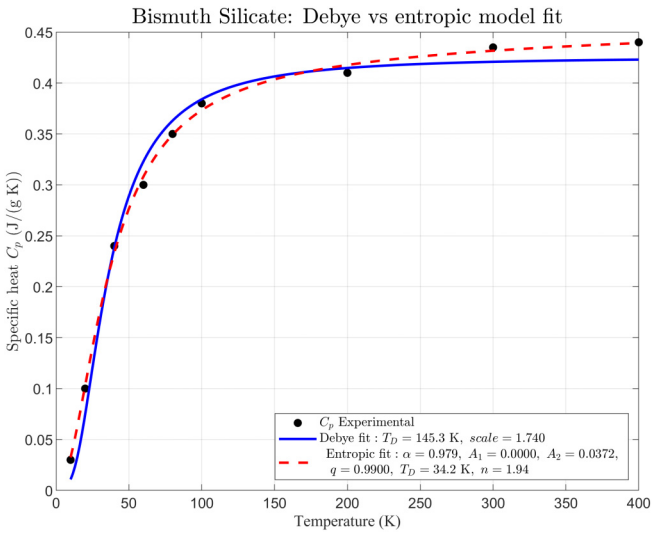


FIG. 9. Specific heat capacity for bismuth silicate: Debye versus entropic model with high-temperature regularization fit. Data from Onderka [72]. The corresponding best-fit parameters are reported in the plot legend.

The systematic analysis of the fitted parameters is summarized in Table I.

Additivity behavior associated with q. All fitted values satisfy $q < 1$, ranging from $q = 0.9339$ for sapphire to $q = 0.9902$ for the cobalt nanowire composite. Within the standard Tsallis composition rule, these values correspond to an effectively superadditive entropy. The departure from the additive Boltzmann–Gibbs limit is relatively weak for most of the materials, whereas sapphire exhibits the largest deviation. These values may reflect effective correlations, structural constraints, interface contributions, phonon confinement, or heterogeneous connectivity. We emphasize, however, that additivity and extensivity are conceptually distinct: extensivity concerns the scaling of entropy with system size and cannot be inferred solely from whether q is smaller or greater than unity [14].

TABLE I. Best-fit parameters for the regularized entropic specific-heat model, Eq. (57). The Co-NW entry denotes the cobalt nanowire composite. Values are quoted to the precision displayed in the corresponding plot legends.

Material	α	A_1	A_2	q	T_D (K)	n
Sapphire	0.734	0.0000	0.0012	0.9339	296.1	1.80
Quartz	1.000	0.0000	0.0317	0.9867	33.6	2.02
Germanium	0.707	0.0000	0.0850	0.9878	35.3	1.70
Bismuth	0.644	0.0000	0.1031	0.9854	33.3	1.67
Antimony	0.826	0.0000	0.0498	0.9843	30.9	1.79
Bismuth silicate	0.979	0.0000	0.0372	0.9900	34.2	1.94
Co-NW composite	0.905	0.0000	0.0030	0.9902	454.6	0.50

Amplitude identifiability. At the reported numerical precision, all fits yield $A_1 = 0.0000$. The fitted expression is therefore effectively governed by

$$C_{V,q}(T) \simeq \frac{B_2 T^{\alpha+1}}{1 + (T/T_D)^n}, \quad B_2 := A_2(1-q). \tag{64}$$

Consequently, the experimental curves primarily constrain the combination B_2 rather than A_2 and q independently. The individual values of A_2 and q should therefore be interpreted with caution unless additional microscopic information or independent constraints are available. In particular, the fitted value of q should be regarded as an effective deformation parameter rather than as a direct and independently measured microscopic quantity.

Effective scaling exponent α. The fitted values lie in the interval $0.644 \leqslant \alpha \leqslant 1.000$. Within the present formulation, α controls the effective power-law dependence of the vibrational contribution. Because the datasets cover different temperature intervals and do not necessarily probe the strict asymptotic low-temperature regime, the fitted α values should be interpreted as effective spectral-scaling exponents associated with the noninteger-dimensional description rather than as direct geometrical measurements of a Hausdorff dimension. Values below the three-dimensional Debye exponent indicate a reduced effective vibrational scaling that may be associated with anisotropy, confinement, interfaces, structural disorder, or departures from the ideal Debye density of states.

High-temperature regularization. Since A_1 is numerically negligible, the high-temperature dependence is controlled by

$$C_{V,q}(T) \sim B_2 T_D^n T^{\alpha+1-n}. \tag{65}$$

For sapphire, quartz, germanium, antimony, bismuth silicate, and bismuth, the fitted values satisfy $n \simeq \alpha + 1$, with $|\alpha + 1 - n| \lesssim 0.07$. Their fitted curves therefore approach a constant or retain only a weak residual temperature dependence at high temperature. This result explains why the regularized expression can reproduce the observed leveling of the specific heat without imposing the exact Dulong–Petit limit as a separate constraint.

The cobalt nanowire composite is an exception, with $\alpha + 1 - n \simeq 1.405$. Its fitted curve therefore remains increasing rather than asymptotically saturating. This behavior is consistent with the limited experimental interval and with the fact that the measured response corresponds to a heterogeneous nanowire composite rather than to a simple bulk crystalline solid. Accordingly, the term *high-temperature regularization* is more appropriate than *saturation* as a universal description of the denominator in Eq. (57).

The fitted crossover scale T_D should likewise be interpreted as an effective model-dependent thermal scale. Germanium, antimony, quartz, bismuth silicate, and bismuth yield values clustered between approximately 31 and 35 K, whereas sapphire and the cobalt nanowire composite yield substantially larger values. These differences reflect both material dependence and the distinct temperature ranges covered by the datasets; they should not automatically be identified with independently measured bulk Debye temperatures.

Taken together, the results establish the descriptive flexibility of the regularized entropic model while also revealing correlations among its fitting parameters. A quantitative microscopic interpretation will require parameter-uncertainty estimates, covariance analysis, and independent experimental or theoretical constraints. The connection to conformable dynamics therefore remains a qualitative microscopic motivation for the deformation rather than a parameter-free determination of q.

The ability of the model to describe different temperature dependencies is consistent with earlier applications of deformed derivative and noninteger-dimensional approaches [20–27].

VII. CONCLUSIONS

We developed a generalized noninteger-dimensional framework for anisotropic solids in which the density of states is modified through the Borges q-deformed derivative. By introducing dimensionless energy and frequency variables, the electronic and phononic constructions remain dimensionally consistent and recover the undeformed noninteger-dimensional results in the limit $q \to 1$.

The resulting regularized entropic specific-heat expression, Eq. (57), was examined using datasets for sapphire, quartz, germanium, antimony, bismuth, bismuth silicate, and a cobalt nanowire composite. Across these systems, the model reproduces the main temperature dependence of the measured specific heat and, in several cases, provides a closer description of the intermediate-to-high-temperature curvature than the Debye benchmark. The improvement is not uniform, however, and the cobalt nanowire composite remains only partially described by either smooth fitting form over the available temperature interval.

The updated parameter set reveals several systematic features. All fitted values satisfy $q < 1$, indicating an effectively superadditive deformation within the standard Tsallis composition rule. With the exception of sapphire, the values remain relatively close to the additive limit. At the reported precision, all fits yield $A_1 = 0.0000$, so the curves are primarily controlled by the effective amplitude $B_2 = A_2(1-q)$. Accordingly, A_2 and q are correlated and should not be regarded as independently determined microscopic observables on the basis of these fits alone.

The fitted exponent α ranges from approximately 0.64 to 1.00. In the present context, it should be interpreted as an effective vibrational scaling exponent associated with the noninteger-dimensional description rather than as a direct geometrical measurement of the material's Hausdorff dimension. Similarly, T_D and n act as effective crossover and regularization parameters and need not coincide with independently measured bulk Debye quantities.

For six of the seven systems, the fitted values satisfy $n \simeq \alpha + 1$. Since A_1 is numerically negligible, this relation produces an approximately constant high-temperature response through the asymptotic dependence $C_{V,q} \sim T^{\alpha+1-n}$. The cobalt nanowire composite is the principal exception and retains a rising fitted response, consistent with its restricted measurement interval and heterogeneous composite character. The denominator in Eq. (57) should therefore be understood as a phenomenological high-temperature regularization rather than as a universal enforcement of the exact Dulong–Petit limit.

The present results demonstrate that the q-deformed noninteger-dimensional model is a flexible phenomenological framework for describing non-Debye specific-heat behavior. They also show that physical interpretation of the individual fitted parameters requires care: parameter correlations, dataset-dependent temperature ranges, and the absence of the strict asymptotic low-temperature regime can all affect the extracted values.

The qualitative connection between the deformation and disorder-controlled conformable kinetics provides a possible microscopic motivation for the model. A quantitative relation between q and a kinetic exponent such as μ, however, remains dependent on the microscopic dynamics and on material-specific calibration. Future work should therefore include covariance and uncertainty analysis, comparison using information criteria, independent constraints on q and α, and a reparameterization in terms of the directly constrained combination $B_2 = A_2(1-q)$. Extensions to thermal conductivity, thermoelectric response, and time-dependent transport may then provide further tests of the framework.

ACKNOWLEDGMENTS

J.W. acknowledges partial financial support from FAPERJ through APQ1. R.M. acknowledges funding from the German Research Foundation (DFG, Grant ID 318763901, CRC 1294). During the preparation of this work, the authors used ChatGPT to improve the English language and readability. After using this tool, the authors reviewed and edited the content as necessary and take full responsibility for the content of the publication.

DATA AVAILABILITY

The code and data used in the figures of this article can be found at this repository [73].

APPENDIX: FITTING PROCEDURE FOR THE DEBYE AND ENTROPIC MODELS

The experimental $C_p(T)$ points for the cobalt nanowire composite were digitized from Fig. 6 of Pradhan *et al.* [17] over the interval 300–400 K. The Debye reference curve was fitted by nonlinear least squares using

$$C_p^{\mathrm{Debye}}(T) = s\,9R\left(\frac{T}{T_D}\right)^3 \int_0^{T_D/T} \frac{x^4 e^x}{(e^x-1)^2}\,dx, \qquad \text{(A1)}$$

with T_D and an overall scale factor s treated as free parameters. Here s is a dimensionless overall scale factor used only in the Debye benchmark fit. It compensates for the amplitude mismatch between the standard Debye heat-capacity expression and the experimentally extracted effective $C_p(T)$ of the cobalt nanowire composite, whose measured response includes composite/sample-cell effects.

The entropic model was fitted over the same temperature interval using nonlinear least squares with model-specific parameter bounds. The Debye fit is shown only as a benchmark reference. Its poor agreement with the data reflects the fact that the extracted dataset corresponds to a nanowire composite with strong composite/interface effects rather than a simple bulk crystalline cobalt sample.

[1] J. M. Ziman, *Electrons and Phonons: The Theory of Transport Phenomena in Solids*, The International Series of Monographs on Physics (Oxford University Press, Oxford, 1960).
[2] N. W. Ashcroft and N. D. Mermin, *Solid State Physics* (Holt, Rinehart and Winston, New York, 1976).
[3] C. Kittel, *Introduction to Solid State Physics*, 8th ed. (John Wiley & Sons, Hoboken, NJ, 2005), p. 704.
[4] K. S. Novoselov, A. Mishchenko, A. Carvalho, and A. H. C. Neto, 2D materials and van der Waals heterostructures, Science **353**, aac9439 (2016).
[5] A. K. Geim and I. V. Grigorieva, Van der Waals heterostructures, Nature (London) **499**, 419 (2013).
[6] P. M. Ajayan, L. S. Schadler, C. Giannaris, and A. Rubio, Single-walled carbon nanotube–polymer composites: Strength and weakness, Adv. Mater. **15**, 750 (2003).
[7] J. N. Coleman *et al.*, Two-dimensional nanosheets produced by liquid exfoliation of layered materials, Science **331**, 568 (2011).
[8] P. Debye, Zur Theorie der spezifischen Wärmen, Ann. Phys. **344**, 789 (1912).
[9] T. Nakayama, K. Yakubo, and R. L. Orbach, Dynamical properties of fractal networks: Scaling, numerical simulations, and physical realizations, Rev. Mod. Phys. **66**, 381 (1994).
[10] A. A. Balandin, Thermal properties of graphene and nanostructured carbon materials, Nat. Mater. **10**, 569 (2011).
[11] S. Alexander and R. Orbach, Density of states on fractals: Fractons, J. Phys. Lett. **43**, 625 (1982).
[12] R. Orbach, Dynamics of fractal networks, Science **231**, 814 (1986).
[13] J. H. He, Anisotropy and isotropy: A model of fraction-dimensional space, Solid State Commun. **75**, 111 (1990).
[14] C. Tsallis, Possible generalization of Boltzmann-Gibbs statistics, J. Stat. Phys. **52**, 479 (1988).
[15] C. Tsallis, *Introduction to Nonextensive Statistical Mechanics* (Springer, New York, 2009).
[16] C. Tsallis, Beyond Boltzmann–Gibbs–Shannon in physics and elsewhere, Entropy **21**, 696 (2019).
[17] N. R. Pradhan, H. Duan, J. Liang, and G. S. Iannacchione, Specific heat and thermal conductivity measurements for anisotropic and random macroscopic composites of cobalt nanowires, Nanotechnology **19**, 485712 (2008).
[18] R. Metzler and J. Klafter, The random walk's guide to anomalous diffusion: A fractional dynamics approach, Phys. Rep. **339**, 1 (2000).
[19] R. Metzler and J. Klafter, The restaurant at the end of the random walk: Recent developments in the description of anomalous transport by fractional dynamics, J. Phys. A **37**, R161 (2004).
[20] J. Weberszpil, M. J. Lazo, and J. A. Helayël-Neto, On a connection between a class of q-deformed algebras and the Hausdorff

derivative in a medium with fractal metric, Physica A **436**, 399 (2015).
[21] O. Sotolongo-Costa and J. Weberszpil, Explicit time-dependent entropy production expressions: Fractional and fractal Pesin relations, Braz. J. Phys. **51**, 635 (2021).
[22] Y. Liang, W. Xu, W. Chen, and J. Weberszpil, From fractal to a generalized fractal: Non-power-function structural metric, Fractals **27**, 1950083 (2019).
[23] J. Weberszpil and J. A. Helayël-Neto, Variational approach and deformed derivatives, Physica A **450**, 217 (2016).
[24] J. Weberszpil and W. Chen, Generalized Maxwell relations in thermodynamics with metric derivatives, Entropy **19**, 407 (2017).
[25] W. Rosa and J. Weberszpil, Dual conformable derivative: Definition, simple properties and perspectives for applications, Chaos Solit. Fractals **117**, 137 (2018).
[26] O. Sotolongo-Costa, J. Weberszpil, and O. Sotolongo-Grau, in *Fractal Signatures in the Dynamics of an Epidemiology* (CRC Press, Boca Raton, FL, 2023), pp. 19–28.
[27] W. Xu, W. Chen, Y. Liang, and J. Weberszpil, A spatial structural derivative model for ultraslow diffusion, Therm. Sci. **21**, 121 (2017).
[28] J. Weberszpil, Microscopic origins of conformable dynamics: From disorder to deformation, Physica A **678**, 130945 (2025).
[29] E. P. Borges, A possible deformed algebra and calculus inspired in nonextensive thermostatistics, Physica A **340**, 95 (2004).
[30] P. Hyldgaard and G. D. Mahan, Phonon superlattice transport, Phys. Rev. B **56**, 10754 (1997).
[31] M. V. Simkin and G. D. Mahan, Minimum thermal conductivity of superlattices, Phys. Rev. Lett. **84**, 927 (2000).
[32] D. W. Schaefer and K. D. Keefer, Structure of random porous materials: Silica aerogel, Phys. Rev. Lett. **56**, 2199 (1986).
[33] N. Rahmani and R. S. Dariani, Porosity-dependent fractal nature of the porous silicon surface, AIP Adv. **5**, 077112 (2015).
[34] R. Metzler, E. Barkai, and J. Klafter, Anomalous diffusion and relaxation close to thermal equilibrium: A fractional Fokker-Planck equation approach, Phys. Rev. Lett. **82**, 3563 (1999).
[35] F. H. Stillinger, Axiomatic basis for spaces with noninteger dimension, J. Math. Phys. **18**, 1224 (1977).
[36] W. Chen, Time-space fabric underlying anomalous diffusion, Chaos Solit. Fractals **28**, 923 (2006).
[37] K. Falconer, *Fractal Geometry: Mathematical Foundations and Applications*, 2nd ed. (John Wiley & Sons, Chichester, UK, 2003).
[38] F. Hausdorff, Dimension und Tauml;ußeres Maß, Math. Ann. **79**, 157 (1918).
[39] A. S. Balankin and B. Mena, Vector differential operators in a fractional dimensional space, on fractals, and in fractal continua, Chaos Solit. Fractals **168**, 113203 (2023).
[40] V. E. Tarasov, Calculus in noninteger-dimensional space: Tool for fractal physics, Fractal Fract. **9**, 714 (2025).
[41] V. E. Tarasov, General fractional calculus in noninteger dimensional space, Bol. Soc. Mat. Mex. **32**, 32 (2026).
[42] V. E. Tarasov, Thermodynamics with non-integer dimensional space of states: Fractality of state set, Chaos Solit. Fractals **209**, 118394 (2026).
[43] A. Sur, Fractal theory of thermoelasticity in noninteger dimension space, Z. Angew. Math. Mech. **105**, e202401301 (2025).
[44] W. Keune, S. Hong, M. Y. Hu, J. Zhao, T. S. Toellner, E. E. Alp, W. Sturhahn, T. S. Rahman, and B. Roldan Cuenya, Influence of interfaces on the phonon density of states of nanoscale metallic multilayers: Phonon confinement and localization, Phys. Rev. B **98**, 024308 (2018).
[45] J. Naudts, *Generalised Thermostatistics* (Springer, London, 2011).
[46] *Nonextensive Statistical Mechanics and its Applications*, edited by S. Abe and Y. Okamoto, Lecture Notes in Physics, Vol. 560 (Springer, Berlin, Heidelberg, 2001).
[47] J. P. Boon and C. Tsallis, Nonextensive statistical mechanics: New trends, new perspectives, Europhys. News **36**, 185 (2005).
[48] R. M. Pickup, R. Cywinski, C. Pappas, B. Farago, and P. Fouquet, Generalized spin-glass relaxation, Phys. Rev. Lett. **102**, 097202 (2009).
[49] F. D. Nobre, M. A. Rego-Monteiro, and C. Tsallis, Nonlinear relativistic and quantum equations with a common type of solution, Phys. Rev. Lett. **106**, 140601 (2011).
[50] A. Deppman, A. K. Golmankhaneh, E. Megías, and R. Pasechnik, From the Boltzmann equation with non-local correlations to a standard non-linear Fokker–Planck equation, Phys. Lett. B **839**, 137752 (2023).
[51] M. S. Reis, J. C. C. Freitas, M. T. D. Orlando, E. K. Lenzi, and I. S. Oliveira, Evidences for Tsallis non-extensivity on CMR manganites, Europhys. Lett. **58**, 42 (2002).
[52] M. S. Reis, J. P. Araújo, V. S. Amaral, E. K. Lenzi, and I. S. Oliveira, Magnetic behavior of a non-extensive *S*-spin system: Possible connections to manganites, Phys. Rev. B **66**, 134417 (2002).
[53] M. S. Reis, V. S. Amaral, J. P. Araújo, and I. S. Oliveira, Magnetic phase diagram for a non-extensive system: Experimental connection with manganites, Phys. Rev. B **68**, 014404 (2003).
[54] F. A. R. Navarro, M. S. Reis, E. K. Lenzi, and I. S. Oliveira, A study on composed non-extensive magnetic systems, Physica A **343**, 499 (2004).
[55] M. S. Reis, V. S. Amaral, R. S. Sarthour, and I. S. Oliveira, Physical meaning and measurement of the entropic parameter q in an inhomogeneous magnetic system, Eur. Phys. J. B **50**, 99 (2006).
[56] M. S. Reis, V. S. Amaral, R. S. Sarthour, and I. S. Oliveira, Experimental determination of the non-extensive entropic parameter q, Phys. Rev. B **73**, 092401 (2006).
[57] D. O. Soares-Pinto, M. S. Reis, R. S. Sarthour, and I. S. Oliveira, Spin-waves in a complex magnetic system: Nonextensive approach, J. Stat. Mech. (2007) P08011.
[58] D. O. Soares-Pinto, N. Crokidakis, A. M. Souza, R. S. Sarthour, M. S. Reis, and I. S. Oliveira, Finite size scaling of a 2D Ising model within a nonextensive approach, Phys. Rev. E **80**, 051101 (2009).
[59] R. K. Pathria and P. D. Beale, *Statistical Mechanics*, 3rd ed. (Elsevier, Amsterdam, 2011).
[60] V. E. Tarasov, Vector calculus in noninteger dimensional space and its applications to fractal media, Commun. Nonlinear Sci. Numer. Simul. **20**, 360 (2015).
[61] V. E. Tarasov, Fractional statistical mechanics, Chaos **16**, 033108 (2006).
[62] V. E. Tarasov, Fractional hydrodynamics equations for fractal media, Ann. Phys. **318**, 286 (2005).

[63] J. Hu, X. Liu, C. L. Yue, J. Y. Liu, H. W. Zhu, J. B. He, J. Wei, Z. Q. Mao, L. Y. Antipina, Z. I. Popov, *et al.*, Enhancing electron coherence via quantum phonon confinement in atomically thin Nb_3SiTe_6, Nat. Phys. **11**, 471 (2015).

[64] C. E. Bottani and D. Fioretto, Brillouin scattering of phonons in complex materials, Adv. Phys.: X **3**, 1467281 (2018).

[65] M. M. Sadeghi, I. Jo, and L. Shi, Phonon-interface scattering in multilayer graphene on an amorphous support, Proc. Natl. Acad. Sci. USA **110**, 16321 (2013).

[66] M. Abramowitz and I. A. Stegun, *Handbook of Mathematical Functions with Formulas, Graphs, and Mathematical Tables*, National Bureau of Standards Applied Mathematics Series, Vol. 55 (Dover Publications, New York, 1964).

[67] I. S. Gradshteyn and I. M. Ryzhik, *Table of Integrals, Series, and Products*, 7th ed. (Academic Press, Burlington, MA, 2007).

[68] D. A. Ditmars, S. Ishihara, S. S. Chang, G. Bernstein, and E. D. West, Enthalpy and heat capacity standard reference material: Synthetic sapphire (alpha-Al_2O_3) from 10 to 2250 K, J. Res. Natl. Bur. Stand. **87**, 159 (1982).

[69] TA Instruments, *Sapphire Specific Heat Capacity Literature Values*, Thermal Analysis Application Note TN-8A (TA Instruments, Inc., New Castle, DE, 2003), accessed April 7, 2026.

[70] U. Piesbergen, Die mittleren Atomwrmen der AIII BVHalbleiter AlSb, GaSb, GaAs, InP, InAs, InSb und die Atomwrme des Elements Ge zwischen 12 und 273 K, Z. Naturforsch. A **18**, 141 (1963).

[71] NIST, NIST chemistry WebBook: Shomate equation, National Institute of Standards and Technology, 2024, https://webbook.nist.gov/.

[72] B. Onderka, The heat capacity of bismuth silicates, Thermochim. Acta **601**, 68 (2015).

[73] https://github.com/metz-lab/q-deformed-fractal-dimension.